IEEE Access
Multidisciplinary | Rapid Review | Open Access Journal

Received June 18, 2020, accepted June 29, 2020, date of publication July 7, 2020, date of current version July 20, 2020.

Digital Object Identifier 10.1109/ACCESS.2020.3007799

A Coupling Dynamic Model for Studying the Physical Interaction Between a Finger Exoskeleton and a Human Finger

YANGWEI WANG, (Member, IEEE), SHUFANG ZHENG, ZHICHENG SONG, JINGQUAN PANG, AND JIAN LI, (Member, IEEE)
College of Mechanical and Electrical Engineering, Northeast Forestry University, Harbin 150040, China

Corresponding authors: Jian Li (lijian@nefu.edu.cn) and Zhicheng Song (849094291@qq.com)

This work was supported in part by the Fundamental Research Funds for the Central Universities under Grant 2572018BF03, in part by the Natural Science Foundation of Heilongjiang Province under Grant LH2019E008, and in part by the National Natural Science Foundation of China under Grant 51905084.

ABSTRACT This paper presents a coupling dynamic model that is based on a spring-damping contact for modeling and analyzing the physical interaction between the soft exoskeleton and the finger. The physiological structure and biomechanical model of the finger were introduced. According to the movement mechanism of the finger, a bionic prototype of the single-finger model, which is driven by shape memory alloy (SMA) wire, was designed, and its mechanical model was established. A spring-damping model was used to expound an interaction force of a human-robot with a coupling dynamic model. The experiment was carried out to verify the exoskeleton mechanical model and determine the bending angle trajectory of each joint. The inverse solution of the coupling dynamic model was verified by using angle data and driving parameters as input. According to the torque relationship, the actual active shrinkage torque of SMA wire was compared with the simulation data for the circumstances with or without consideration of the interaction contact force. The results confirm that the actual values are consistent with the simulation values. After comparing the actual active shrinkage torque and simulation curve without considering the interaction contact force, the error range is between 0 and 19.57 N · mm. The comparison that considers the interaction contact force model yields an error range between −0.74 and 10.89 N · mm. The accuracy of the model is increased by an average of 7.05%.

INDEX TERMS Hand rehabilitation exoskeleton, SMA wire, interaction contact force, coupling dynamic.

I. INTRODUCTION

Stroke is a disease that seriously endangers human health and can cause various types of nerve damage or even lead to death. Approximately 80% of stroke survivors will lose their ability to live independently and may even have permanent disability, which will seriously affect their mental health and quality of life. The hand is the most important sensory organ of humans. Stroke will have a great influence on the movement mechanism of the hand after nerve damage. According to the data, six months after experiencing a stroke, 65% of patients lost their hand function and could not perform daily operations [1]. They need rehabilitation training to improve hand function.

With the continuous development of robot technology, many researchers have carried out exploratory research on hand function rehabilitation robots and exoskeleton movement function models. A hand motion-assisted rehabilitation robot was designed by Gifu University. The robot was driven by a connecting rod to realize the rehabilitation movement of the finger [2]. A pneumatic manual rehabilitation robot was designed by Tokyo Institute of Technology, which employed pneumatic artificial muscles to drive the structure. Electromyogram signals were introduced into the motion control of the rehabilitation robot to achieve the rehabilitation function of the finger [3]. Using a motor and cylinder as the driving source, most joints are rigidly connected in

The associate editor coordinating the review of this manuscript and approving it for publication was Yingxiang Liu.

an exoskeleton structure, which aggravates its complexity. Therefore, the Exo-Glove Poly II soft wearable rehabilitation glove, which is driven by rope, was designed by Seoul University to realize bending movement [4]. A prototype of the wearable rehabilitation glove driven by shape memory alloy wire has been developed by Tehran University [5]. SMA wire was employed to pull a cable and drive a single finger to achieve flexion and extension. The experimental results show that the output force of a single finger is approximately 10 N, which can satisfy the daily grip requirement. In recent years, the major driving ways of an exoskeleton robot are rope driving [6]–[8] and pneumatic driving [9], [10].

To achieve control of an exoskeleton, it is necessary to establish a dynamic model to control the output torque. A finger rehabilitation training device was developed by YanShan University [11]. The device relied on a motor to pull a rope to realize flexion and extension. In the research, the Lagrange equation was applied to analyze the dynamic of finger rehabilitation training device, and a dynamic model was established. A rehabilitation exoskeleton robot of pneumatic artificial muscle was developed by Dong Eui University [12]. Based on the displacement function of a piston, a second-order differential equation was established, and the relationship between the output pressure and the displacement of the piston was solved. According to the geometric relationship of the exoskeleton, the corresponding theoretical bending angle was calculated. Harbin Institute of Technology has investigated the rehabilitation exoskeleton robot based on a variety of position sensors and pressure sensors [13] and attempted to establish an exoskeleton mechanics model based on the principle of statics. It is determined that most of the trajectory of a hand rehabilitation exoskeleton robot is designed based on the movement function of the finger and the variation in the contact force between the finger and the exoskeleton is seldom considered in the process of movement. In the field of hand rehabilitation exoskeleton robots, there is a lack of appropriate coupling dynamic model.

First, according to the physiological structure and movement mechanism of the finger, a principle prototype of a single-finger driven by SMA is designed with the established mechanical model. Second, to fully consider the interaction between the finger and the exoskeleton, an interaction contact force model is established and coupled with the muscle force, mechanical model and finger dynamic equation. Last, the coupling dynamic model is verified by comparing the simulation curve and the actual curve to improve the accuracy of the dynamic model.

II. PHYSIOLOGICAL STRUCTURE OF FINGER

A. MOVEMENT MECHANISM OF FINGER

A finger joint can be regarded as an ideal rigidity structure joint. The index finger, as an example, mainly consists of three phalanges: the distal phalange, middle phalange, and proximal phalange. The joint between the distal phalange and the middle phalange is referred to as the DIP joint. The joint between the middle phalange and the proximal phalange is referred to as the PIP joint. The joint between the proximal phalange and the metacarpal skeleton is referred to as the MCP joint [14]. The DIP and PIP joints have only one freedom that can achieve the extension and flexion of the finger. The MCP joint has two freedoms that can realize the extension and flexion of the finger or the abduction and adduction of the finger. The movement of the finger is mainly coordinated by six muscles, four tendons and ligaments (refer to Figure 1). The six muscles include the Flex Digitorum Profundus (FDP), Flex Digitorum Superficialis (FDS), Long Extenor (LE), Radial Interosseous (RI), Ulnar Interosseous (UI), and Lumberic (LU); the four tendons include the Terminal Extractor (TE), Extractor Slip (ES), Ulnar Band (UB) and Radial Band (RB) [15]. The muscle force is generated by the six muscles and transmitted to the phalangeal joint via a complex tendon network to balance the external contact force. The starting point of the muscles differs. In anatomy, these muscles can be divided into vitro muscles and vivo muscles. The FDP, FDS and LE belong to the vitro muscles and are connected to the skeleton of the finger by long tendons. The main function of the vitro muscles is to complete the functional operation. The vivo muscles are directly connected to the skeleton; their main function is to restrain the joints. The extensors constitute a complex tendon network, which transmits the force produced by the muscle to the joints. The TE is mainly responsible for the stretch of the DIP joint in the front of the middle phalanx. The TE is divided into two tendons: the UB and RB. The TE can transfer the force to the UB and RB for the stretch of the PIP joint. The ES is also distributed in the middle phalanx. The PIP and MCP joints are stretched with the ES and LE simultaneously compressed. The LU connects the LE and FDP and has the same function as the UI and RI. The LU is mainly utilized to complete the abduction and adduction of the finger. According to the analysis, the FDP and FDS are responsible for the bending movement of the finger. The TE, ES and LE are responsible for the extension and flexion movement of the finger. The RI, UI, and LU are responsible for not only for the extension and flexion movement of the finger but also the abduction

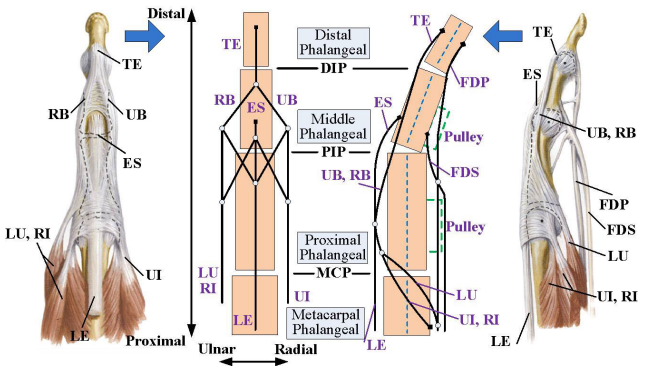

FIGURE 1. Movement mechanism of finger.

and adduction movement. The physiological structure and movement mechanism of the finger is shown in Figure 1.

B. MUSCLE MECHANICS

The finger muscles and tendons of healthy people are very flexible and cannot cause increased resistance for finger bending. However, stroke patients' finger muscles and tendons are very stiff because of multiple nerve damage, which will produce great resistance for the bending movement.

In this paper, the hand of the experimenter, who does not present any disease, is applied for research. The Hill model is usually employed to solve the finger muscle force, which is mainly composed of the Contractile Element (CE), Parallel Elastic Element (PEE) and Series Elastic Element (SEE) [16]. The Hill model is shown in Figure 2.

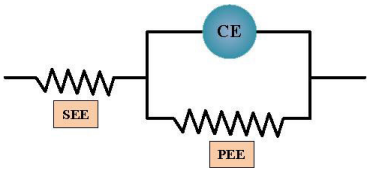

FIGURE 2. Hill model.

The CE and PEE belong to muscle tissue fibers, while the SEE is considered a tendon. Because the tendon is inelastic, the SEE is often disregarded by many researchers. The CE is produced by active muscle shrinkage under nerve stimulation. In rehabilitation training, the finger is in a passive bending state. The muscle force only depends on the PEE, and the force produced by the CE can be regarded as zero. In this case, the equation of the Hill model is

$$F_{Muscle} = F_{PEE} = F_o \cdot fl_{PEE} \tag{1}$$

where F_o is the maximal isometric force, and fl_{PEE} is the length factor of passive parallel element.

fl_{PEE} can be expressed as a piecewise function.

$$fl_{PEE} = \begin{cases} 0 & l_N \le 1 \\ \left(\exp\left(\dfrac{k_{pe} \cdot (l_N - 1)}{e_o}\right) - 1\right) / \left(\exp\left(k_{pe}\right) - 1\right) & l_N > 1 \end{cases} \tag{2}$$

where k_{pe} represents the curve shape factor, e_o is the passive factor of muscle in the maximal isometric and l_N is the normalized muscle length. The k_{pe} value of young people is 5, and that of old people is 4. The e_o value is 0.6 for young people and 0.5 for old people [17].

l_N satisfies the following relationship.

$$l_N = \frac{l_f}{l_o} \tag{3}$$

where l_f is the tendon slack length, and l_o is the optimal fiber length.

By substituting equation (2) and (3) into equation (1), the impedance force of the finger muscle can be calculated.

In the process of finger bending assisted by the exoskeleton, the main muscle impedance force is derived from the LE. Due to the difference in the physiological parameters of the finger, the reference values of the F_o, L_o and L_f of the human index finger muscles in a healthy state can be obtained by reviewing studies. The data results are shown in Table 1.

TABLE 1. Reference data of index finger physiological parameters.

Literature	Muscle	F_o(N)	L_o(cm)	L_f(cm)
[18]	*LE*	18.3	7.0	32.2
[19]	*LE*	13.8	7.0	38.5

Considering the mean value of the data and using MATLAB software, an LE value of 0.1082 N is obtained. This finding shows that the muscle passive impedance of the finger in a healthy state is very small. The result is consistent with the actual circumstance.

III. DESIGN AND MECHANICAL ANALYSIS OF THE SINGLE-FINGER BIOMIMETIC STRUCTURE

A. BIOMIMETIC STRUCTURE

The index finger is considered as an example. According to the movement mechanism of the finger, the extensor and flexor of the finger are simplified into two long tendons. Thermoplastic Polyurethanes (TPU) is selected as exoskeleton material. The tensile strength and bending strength of this material are 18 MPa and 6.2 MPa respectively. It has high mechanical properties and better elasticity, so it is very suitable as an exoskeleton material. The prototype consists of the TPU exoskeleton, arm bracket, pulleys, pressure sensor, flexible pressure sensor and two 0.3 mm SMA wires. The exoskeleton is continuously bent by the shrinkage force of SMA wire. The SMA wires are symmetrically arranged on the upper and lower sides of the exoskeleton to simulate the extensor and flexor of the finger. One side of the SMA wire is fixed in the fingertip sheath, and the other side of the SMA wire is fixed in the pull rod after repeatedly coiled pulleys. SMA wire passive tension data are collected by using a pressure sensor. The pressure senor, which is referred to a NLBS-VLL-5kg produced by ZhongNuo Senor Company in China, is selected with the range of accuracy of 0 to 50 N and 0.1 N. To measure the human-machine interaction contact force between the finger and the exoskeleton, a flexible pressure sensor is installed in the contact area between the finger and the exoskeleton. The Flexiforce flexible sensor, which is constructed in America, is selected with the range of accuracy of 0 to 110 N and ±3% linearity. The structure principle is shown in Figure 3 (a, b), and the exoskeleton prototype is shown in Figure 4 (a, b).

B. MECHANICAL MODEL

When the finger is bent, the SMA wire of the hand palm side is heated to generate active shrinkage tension, and the

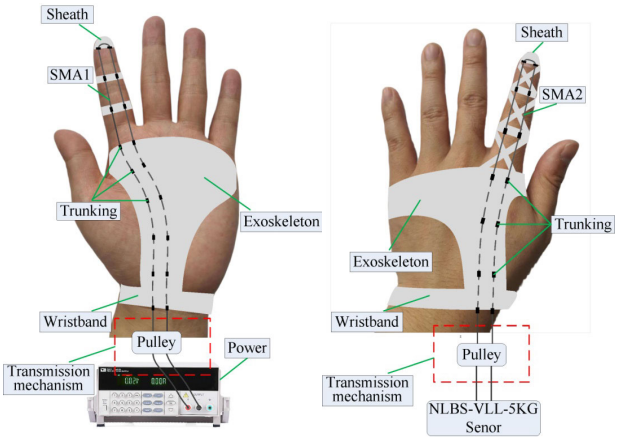

(a) hand, palm side (b) hand, back side

FIGURE 3. .Structure principle of single-finger rehabilitation skeleton.

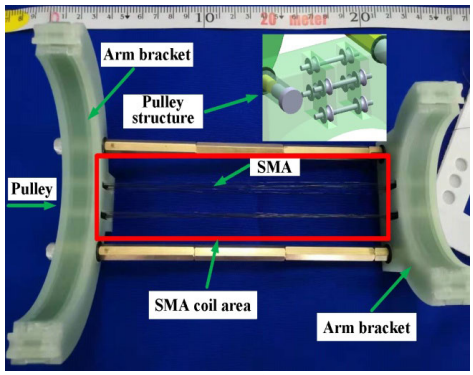

(a) Arm bracket structure

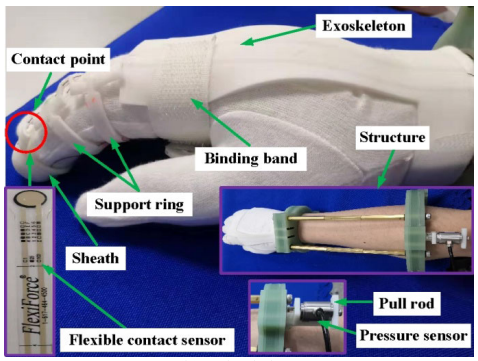

(b) Principle prototype

FIGURE 4. Prototype of single-finger rehabilitation exoskeleton.

SMA wire of the hand back side is heated to generate passive tension. Simultaneously, the human-machine interaction force between the exoskeleton and the finger cannot be disregarded. The contact point between the experimenter's index finger and the exoskeleton is located at the dorsal position of the fingertip. This positioning promotes the effect of index finger bending.

According to this analysis, the principle virtual work principle is applied to obtain the following relation. The mechanical model is shown in Figure 5.

$$\vec{F_{SMA1}} \cdot \delta \vec{\mu}_1 + \vec{F_{SMA2}} \cdot \delta \vec{\mu_2} + \vec{F_c} \cdot \delta \vec{x} = 0 \tag{4}$$

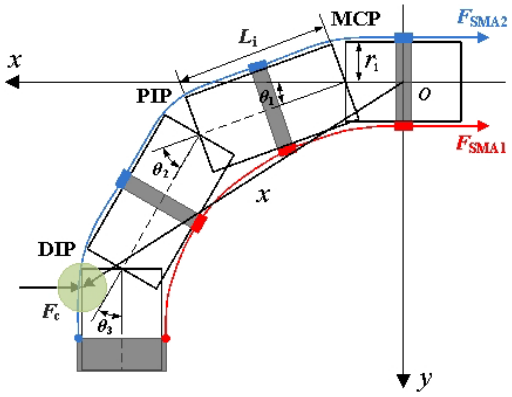

FIGURE 5. Principle prototype of single-finger mechanical model.

where $\vec{F_{SMA1}}$ and $\vec{F_{SMA2}}$ represent the force of SMA, and $\vec{F_c}$ is the interaction force. $\delta \vec{\mu_1}$, $\delta \vec{\mu_2}$ and $\delta \vec{x}$ represent the corresponding virtual displacements.

For the solution of $\delta \vec{\mu_1}$ and $\delta \vec{\mu_2}$, the rotation joint is regarded as a circle. According to establishing the X-Y coordinate system and geometric relation, the following relation can be obtained.

$$\vec{\mu} = -(r_1 \cdot \theta_1 + r_2 \cdot \theta_2 + r_3 \cdot \theta_3)\hat{i} \tag{5}$$

where r_1, r_2 and r_3 represent the circle radius, and θ_1, θ_2 and θ_3 are the joint angles.

Similarly, the position vector $\vec{x}$ can be expressed as:

$$\begin{aligned}\vec{x} = {} & (L_1\cos(\theta_1) + L_2\cos(\theta_1+\theta_2) + L_3\cos(\theta_1+\theta_2+\theta_3))\hat{i} \\ & + (L_1\sin(\theta_1) + L_2\sin(\theta_1+\theta_2) + L_3\sin(\theta_1+\theta_2+\theta_3))\hat{j}\end{aligned} \tag{6}$$

where L_1, L_2 and L_3 represent the phalangeal length.

The force vectors $\vec{F_{SMA1}}$, $\vec{F_{SMA2}}$ and $\vec{F_{SMA2}}$ can be expressed as follows:

$$\vec{F_{SMA}} = -|F_{SMA}|\hat{i} \tag{7}$$

$$\vec{F_c} = -|F_c|\sin(\theta_1+\theta_2+\theta_3)\hat{i} + |F_c|\cos(\theta_1+\theta_2+\theta_3)\hat{j} \tag{8}$$

Based on the coupling relationship of each joint, there are the following relationship equations [20].

$$\begin{cases} \theta_2 = \dfrac{6}{5}\theta_1 \\ \theta_3 = \dfrac{2}{3}\theta_2 = \dfrac{4}{5}\theta_1 \end{cases} \tag{9}$$

In this analysis, the mechanical model is completed.

As shown in Figure 5, passive tension is generated by SMA2 wire:

$$F_{SMA2} = E_M \varepsilon_{SMA} \cdot \pi r_{SMA}^2 \tag{10}$$

where E_M is the elastic modulus of martensite, ε_{SMA} is the strain and r_{SMA} is the radius of SMA.

Using the strain calculation method of SMA wire, the strain can be determined according to the following geometric relationship.

$$\varepsilon_{SMA} = \frac{r_1\theta_1 + r_2\theta_2 + r_3\theta_3}{l_{SMA}} \tag{11}$$

where l_{SMA} is the initial length of the SMA wire.

The mechanical model of the exoskeleton is completed. However, the active shrinkage tension produced by SMA1 can be solved by the constitutive mode. The essence of the constitutive model is related to its phase transition temperature.

IV. DRIVING ANALYSIS OF SMA WIRE

A. ELECTRIC HEATING MODEL OF SMA WIRE

The corresponding stress and strain of the SMA wire are changed under the phase-transforming temperature. The heating of the SMA wire is controlled by the pulse width modulation (PWM) mode, and then the bending motion of the exoskeleton is controlled. Thus, the electric heating equation of the SMA wire can be obtained [21].

$$mc\frac{dT(t)}{dt} = \frac{U^2}{R}\tau - hA(T(t) - T_0) \tag{12}$$

where l_{SMA} is the PWM ratio; $m = \rho_{SMA}\pi r_{SMA}^2 l_{SMA}$ is the mass of the SMA wire; ρ_{SMA} is the SMA wire density; c is the specific heat; U is the voltage; $R = \rho_{R\_SMA} l_{SMA} / \pi r_{SMA}^2$ is the resistance of the SMA; ρ_{R_SMA} is the resistivity; h is the heat convection coefficient; $A = 2\pi r_{SMA} l_{SMA}$ is the heat transfer area of the SMA wire and T_0 is the ambient temperature.

$$h = h_1 + h_2 \times T(t)^2 \tag{13}$$

where h_1 and h_2 are heat transfer coefficients.

B. CONSTITUTIVE MODEL OF SMA WIRE

The variation in the SMA temperature produces changes in the SMA wire stress and strain during the phase transition. The Tanaka constitutive model describes the corresponding relationship of each parameter as follows [22]:

$$\dot{\sigma} = E\dot{\varepsilon}_{SMA} + \Theta\dot{T} + \Omega\dot{\xi} \tag{14}$$

$$E = E_A + \xi(E_M - E_A) \tag{15}$$

The percentage of martensite in the transition from martensite to austenite is

$$\xi = \frac{1}{2}\{\cos[a_A(T - A_s) + b_A\sigma] + 1\} \tag{16}$$

where A_s is the start temperature of the austenite phase transition; M_s is the start temperature of the martensite phase transition; T is the temperature of the SMA wire; ξ is the percentage of martensite; σ is the stress of the SMA wire; E is the elastic modulus of the SMA phase transition; E_A is the elastic modulus of SMA austenite; Ω is the phase transition coefficient; and the parameters a_A and b_A are defined as:

$$\begin{cases} a_A = \dfrac{\pi}{A_s - A_f} \\ b_A = -\dfrac{a_A}{C_A} \end{cases} \tag{17}$$

where C_A is an austenite transformation coefficient. The performance parameters of SMA are shown in Table 2.

TABLE 2. Performance parameters of SMA wire.

Parameter	Description	Value
l_{SMA}	Initial length of SMA (mm)	1800
r_{SMA}	Radius of SMA (mm)	0.15
c	Specific heat (J/(kg × °C))	870
A_s	Austenite start temperature (°C)	66
A_f	Austenite final temperature (°C)	78
E_M	Elastic modulus of martensite (GPa)	27
E_A	Elastic modulus of SMA austenite (GPa)	65
Θ	Thermoelastic coefficient (MPa / °C)	0.55
C_A	Austenite transformation coefficient (MPa / °C)	13.6×10^6
ε_L	Maximum residual strain	0.067

V. HUMAN-MACHINE COUPLING DYNAMICS MODEL

Before modeling, the following hypothesis must be explained according to the actual situation. (1). The force transfer of SMA wire needs to be realized by pulley, and its resistance is small. The friction loss is not studied here. (2). Grasping action of finger is mainly flexion and extension movement. Consequently, we only consider the sagittal movement and ignore the coronal movement. (3). In the process of bending, the experimenter's finger is only passively bent without any active action. The TPU is selected as the material of the exoskeleton, which has elasticity as a soft material. Therefore, the interaction force between human and machine in the bending process can be simplified as an elastic force for analysis. It is assumed that the stiffness coefficient at the contact point of the exoskeleton and finger is k, and there is a damping effect, whose value is c. The centroid position of the exoskeleton is the same as that of the experimenter's finger. The D-H parameter method is employed to establish the base coordinate system $\{x_oOy_o\}$, the experimenter coordinate system $\{x_sOy_s\}$ and the exoskeleton coordinate system $\{x_eOy_e\}$. The coupling dynamics model is shown in Figure 6.

According to the analysis, the function relationship among the elastic interaction force, elastic coefficient, damping, distance and velocity is established as:

$$\left|{}^sF_{es}\right| = k \cdot \left|{}^sq_{ces}\right| + \dot{c} \cdot \left|{}^s\dot{q}_{ces}\right| \tag{18}$$

where ${}^sq_{ces}$ is the displacement of the exoskeleton contact point c_e and the experimenter's joint contact point c_s in the experimenter's coordinate system, and ${}^s\dot{q}_{ces}$ is the corresponding velocity description.

$${}^sq_{ces} = {}^sq_{ce} - {}^sq_{cs} \tag{19}$$

The displacement should be calculated in the experimenter's coordinate system, and the exoskeleton and

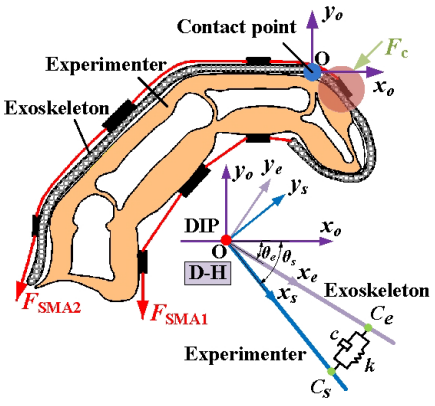

FIGURE 6. Coupling dynamics model.

experimenter share the same base coordinate. Therefore, the position coordinates of the exoskeleton contact point can be transformed into the description for the base coordinate. The calculation is expressed as:

$$ {}^{s}q_{ce} = {}^{s}_{o}T_{s}\,{}^{o}_{e}T_{e}\,{}^{e}q_{ce} \tag{20}$$

where ${}^{s}q_{ce}$ represents the exoskeleton contact point coordinate in the experimenter coordinate system. ${}^{e}q_{ce}$ is the description of the exoskeleton contact point coordinate in the exoskeleton coordinate system. ${}^{o}_{e}T_{e}$ is the homogeneous transformation matrix of the exoskeleton relative to the base coordinate system, and ${}^{s}_{o}T_{s}$ is the homogeneous transformation matrix of the base coordinate system relative to the experimenter coordinate system.

The coordinate form of ${}^{e}q_{ce}$ is expressed as:

$$ {}^{e}q_{ce} = [\,c_e \quad 0 \quad 0\,]^T \tag{21}$$

where ${}^{e}q_{ce}$ is the coordinate of the exoskeleton's centroid, and all joint torsion angles are zero. The coordinate transformation matrix from the exoskeleton coordinate system to the base coordinate system is expressed as follow:

$$ {}^{o}_{e}T_{e} = \begin{bmatrix} \cos\theta_e & -\sin\theta_e & 0 & 0 \\ \sin\theta_e & \cos\theta_e & 0 & 0 \\ 0 & 0 & 1 & 0 \\ 0 & 0 & 0 & 1 \end{bmatrix} \tag{22}$$

The coordinate transformation matrix from the experimenter's coordinate system to the base coordinate system is expressed as follows:

$$ {}^{o}_{s}T_{s} = \begin{bmatrix} \cos\theta_s & -\sin\theta_s & 0 & 0 \\ \sin\theta_s & \cos\theta_s & 0 & 0 \\ 0 & 0 & 1 & 0 \\ 0 & 0 & 0 & 1 \end{bmatrix} \tag{23}$$

$$ {}^{s}_{o}T_{s} = {}^{o}_{s}T_{s}^{-1} = \begin{bmatrix} \cos\theta_s & \sin\theta_s & 0 & 0 \\ -\sin\theta_s & \cos\theta_s & 0 & 0 \\ 0 & 0 & 1 & 0 \\ 0 & 0 & 0 & 1 \end{bmatrix} \tag{24}$$

The transformed homogeneous coordinate is expressed as follow:

$$ {}^{s}q_{ce} = \left[\, c_e\cos(\theta_e-\theta_s) \quad c_e\sin(\theta_e-\theta_s) \quad 0 \quad 1 \,\right]^T \tag{25}$$

The experimenter's contact point coordinate in the experimenter's coordinate system is expressed as follow:

$$ {}^{s}q_{cs} = [\,c_s \quad 0 \quad 0\,]^T \tag{26}$$

The expression is presented as follow:

$$ {}^{s}q_{ces} = \left[\, c_e\cos(\theta_e-\theta_s)-c_s \quad c_e\sin(\theta_e-\theta_s) \quad 0 \,\right]^T \tag{27}$$

The expression for ${}^{s}\dot{q}_{ces}$ is presented as follow:

$$ {}^{s}\dot{q}_{ces} = \left[\, -c_e\sin(\theta_e-\theta_s)(\dot{\theta}_e-\dot{\theta}_s) \quad c_e\cos(\theta_e-\theta_s)(\dot{\theta}_e-\dot{\theta}_s) \quad 0 \,\right]^T \tag{28}$$

In combination with equation (18), equation (27) and equation (28), the value of the contact force can be calculated. The index finger is regarded as a connecting rod, and the centroid is located at the center of each joint. Due to it is difficult to obtain the mass of index finger phalanges, we found an experimenter with his phalanges length similar to that in [23] that the length of proximal phalanx is 46 mm, the middle phalanx is 28 mm, and the distal phalanx is 20 mm. Therefore, the data of phalanx mass in the literature are selected for subsequent calculations. The length and mass data of the experimenter's three phalanges are shown in Table 3.

TABLE 3. Length and mass parameters of experimenter's index finger.

Joint name	Length(mm)	Mass(g)
Proximal phalange	48	125
Middle phalange	28	60
Distal phalange	21	40

The expression of the coupled dynamic model is obtained by using the Lagrange equation as:

$$ M(\theta)\ddot{\theta} + C(\theta,\dot{\theta}) + G(\theta) = T_{SMA1} + T_c - T_{SMA2} - T_{Muscle} \tag{29}$$

where θ represents the generalized coordinates of the joint angle, $M(\theta)$ is the mass matrix, $C(\theta,\dot{\theta})$ is the centripetal force vector, the Coriolis force coupling vector, $G(\theta)$ is the gravity vector and T is the torque.

VI. RESULTS AND DISCUSSION

A. BENDING EXPERIMENT OF THE SINGLE-FINGER REHABILITATION EXOSKELETON

The difference voltage can affect the bending effect of the exoskeleton. Excessive driving voltage can increase the response speed of the SMA wire and improve the temperature of the SMA wire, which causes the material to become overheated. For a long time, the life span of the SMA wire will be reduced. Low voltage may cause insufficient stress on the SMA wire, and the bending effect could not be achieved, or the response time may increase and fail to satisfy the requirement of rehabilitation frequency. According to data, the operating frequency of the rehabilitation is five times per minute [24]. In numerous repeated experiments, it is

confirmed that the most suitable voltage for the exoskeleton robot is 32V. When the voltage is 32V, only 5s is needed to complete a bending movement, which fully satisfies the rehabilitation requirement. Therefore, the voltage of 32 V will be chosen in subsequent experiments and theoretical model calculations.

The exoskeleton was worn on the index finger of the experimenter. The SMA wire of the extensor side is driven. A white glove was worn as insulation to prevent scald caused by electric heating of the SMA wire in the bending experiment, in which the experimenter's finger is in the natural straightening state. In the whole bending process, an industrial CCD camera which produced JHSM500f by JingHang Company in China is utilized to record video, which is processed every 4 frames. The angle values are recorded by connecting marked points on the finger joints. The maximum bending angle is shown in Figure 7. The bending deformation process image sequence of the exoskeleton, while voltage is 32V, is shown in Figure 8.

As shown in figure 7, the maximum bending angle of the MCP joint is 37.5°, the maximum bending angle of the PIP joint is 42°, and the maximum bending angle of the DIP joint is 29.5°. The experimental values are compared with the MATLAB simulation values; the results are shown in Figure 9.

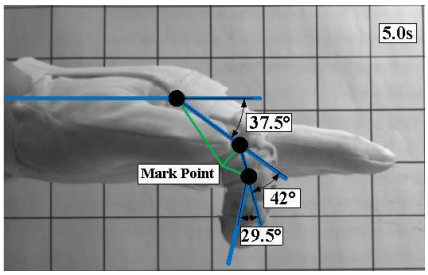

FIGURE 7. Maximum bending state of exoskeleton.

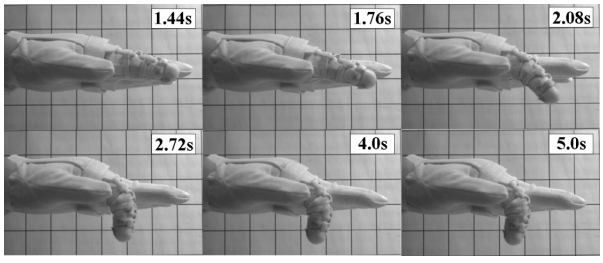

FIGURE 8. Bending deformation process image sequence of exoskeleton for 32 V.

Before the austenite transformation point, the bending angle is not obvious. After the transformation point, the metallographic structure is changed. Martensite gradually transform into austenite, and the joint angle is obviously bent. Before the end temperature of austenite transformation is not reached, the heating power is consistent with the dissipation power, the temperature is not increased, and the bending angle tends to be stable. It can be seen from Figure 9 that the experimental curve is more consistent with the simulation curve and the previously mentioned coupling relationship of the joint. It can be claimed that this difference may be due to the angle collection error and approximation of the joint geometry by a circle.

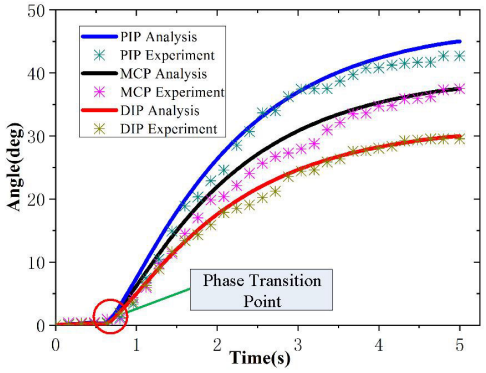

FIGURE 9. Comparison of experiment and simulation.

B. EXPERIMENT OF PWM RATIO AND BENDING ANGLE

The SMA wire is heated by using a constant PWM ratio. When the heating time is sufficient, a different PWM ratio will have a different influence on the phase variables of the SMA wire, which affects the bending angle of the exoskeleton. Due to the coupling relationship among the three joints of the finger, the MCP joint is only analyzed here.

Experiments were carried out to study the relationship between the bending angle and the PWM ratio. The driving voltage was chosen to be 32 V, and the PWM ratio was increased from 0.4. At each duty ratio, a sufficient heating time is required to achieve thermal equilibrium of the SMA wire. According to the theoretical analysis, there is a linear relationship between the PWM ratio and the MCP joint angle. This relationship shows that the analysis curve is consistent with the experiment curve. The experiment data show that the control of the exoskeleton, between 0.4 and 1, can be achieved by a change in the PWM ratio. The maximum bending angle has an approximately linear increase with an increase in the PWM ratio. The relationship between the bending angle PWM ratio and the PWM ratio is shown in Figure 10.

In this part, the appropriate driving parameters are determined. By the analysis of these experiments, the mechanical model is verified. These experimental results can provide data support for the subsequent coupling dynamics model.

C. DETERMINATION OF DYNAMIC PARAMETERS

In this paper, the inverse dynamics are verified. Before analysis, the unknown parameters in the model should be determined. First, according to the angle curve obtained from the mechanical model, the curve of angular velocity and acceleration is determined. The angular velocity and acceleration curve of three joints are shown in Figure 11.

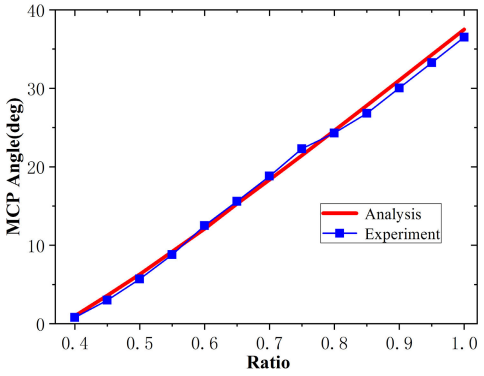

FIGURE 10. Relationship between bending angle and PWM ratio.

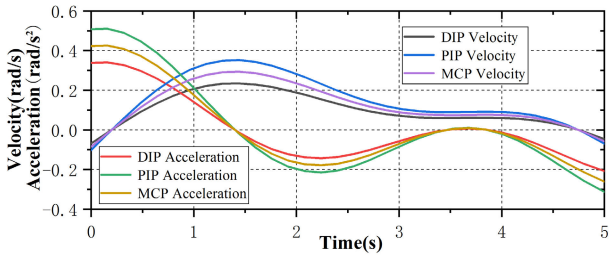

FIGURE 11. Angular velocity and acceleration curve.

Second, for the Human-Machine interaction force equation, the elastic coefficient k and damping coefficient c should be determined. According to the equation of the interaction force, multiple linear regression is used to identify it. Before multiple linear regression, descriptive statistics should be carried out for using the interaction force data samples collected by the Flexiforce sensor. Descriptive statistics are shown in Table 4.

TABLE 4. Sample descriptive statistics.

Variables	Samples	Mean	Std. d	Min	Max
Interaction Force (N)	32	0.902 6762	0.46725 27	0.2	1.47857
Displacement (mm)	32	1.220 969	0.19794 12	0.8192	1.4543
Velocity (mm/s)	32	0.770 2906	0.62208 37	0.1064	2.2763

The regression equation obtained by using Stata/SE15.1 is expressed as follow:

$$y = 0.9815122x_1 - 0.3732791x_2 \tag{30}$$

The regression equation analysis shows that the value of k is 0.9815122N/mm and the value of c is −0.3732791N/(mm/s). The notable probability value of the displacement is 0.009%, and that of the velocity is 0.013%. At the 95% confidence interval, the regression coefficient is significantly different from zero, which indicates that the regression coefficient is reliable. The multiple mutual linear problem cannot be disregarded. The regression equation is checked with the value of the Variance Inflation Factor (VIF) in the Stata/SE15.1. According to experience, when the VIF > 10, the regression equation is considered to have serious multiple mutual linearity. After calculation, the VIF value is 1.05, and there is no multiple mutual linear effect.

The analysis of the interaction contact force, displacement and velocity relationship is shown in Figure 12. The larger is the value of displacement, and the smaller is the velocity, the greater the interaction contact force will be.

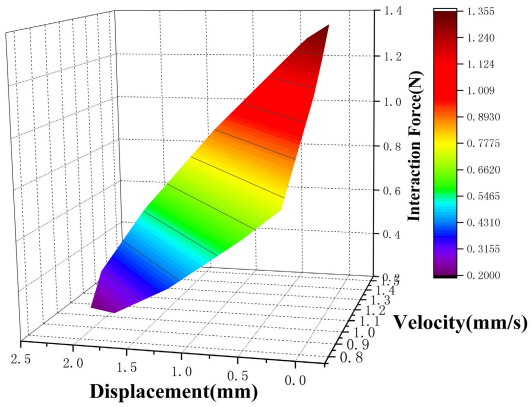

FIGURE 12. Interaction force versus displacement and velocity.

The passive tension is verified by experiments. Using three joint angle curves as the input condition. By substituting equation (11) into equation (10), the passive tension of the SMA wire can be calculated. The experimental values are collected by the pressure sensor. The comparison between the experimental values and the simulation values is shown in Figure 13.

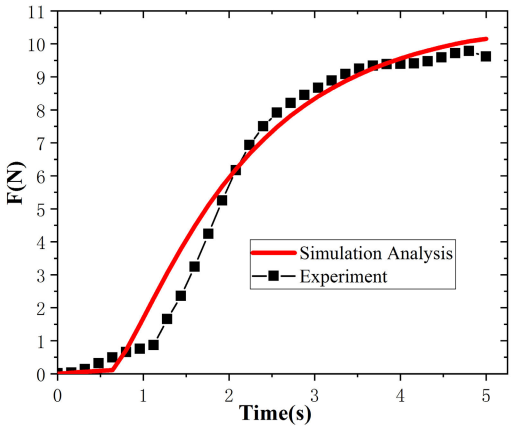

FIGURE 13. Comparison of experimental values and simulation values.

The microstructure of the SMA wire in the cold state, is all martensite. The modulus of elasticity and its radius in the martensitic state are constant. In the process of finger bending, the passive tension is only related to the strain of the SMA wire. The rotation radius of the three joints

and the original length of the SMA wire remain unchanged. The strain value is related to the trajectory of the three joints, and the tension curve should be the linear superposition of the trajectory curves of the three joints. It can be seen from the curve comparison that the simulation curve is more consistent with the experiment curve. Due to the hysteresis of the SMA wire, the experimental phase transition value slightly lags behind the simulation value.

D. COUPLING DYNAMICS ANALYSIS

To verify the coupling dynamic model, it is necessary to determine the driving torque of each joint, which is also the resultant torque of each joint. The dynamics parameters are determined by the experiments, as shown in Table 5.

TABLE 5. Performance parameters of SMA wire.

Parameter	Description	Value
U	Voltage(V)	32
τ	PWM ratio	1
T_0	Ambient temperature (°C)	23
ρ_{SMA}	Density (kg / m^3)	6.5×10^3
ρ_{R_SMA}	Resistivity ($\Omega\cdot$m)	0.32×10^{-6}
h_1	Heat transfer coefficient	300
h_2	Heat transfer coefficient	0.02

Consider the angle simulation curve as the input condition. The driving torque is calculated by MATLAB. The simulation curve of the joint driving torque is shown in Figure 14.

In the sagittal plane, the direction of the finger is regarded as negative when it performs the bending movement. It can be seen from figure 14 (a, b, c) that the driving torque curve of the three joints is negative, and the torque direction is consistent with the actual movement direction. The absolute values of the driving torque of the three joints all show a trend of 's' type reduction, which indicates that when the exoskeleton drives the finger to bend, the torque value in the start-up stage is the maximum. The maximum torque of DIP, PIP and MCP joints were obtained at 0.32s, 0.48s and 0.16s respectively. As the SMA wire reaches the thermal equilibrium state, the active torque tends to be gentle gradually. After 4.5s, terminal (DIP) joint torque tends to zero. It indicates that the movement reached the equilibrium state which this corresponds to the actual movement.

Currently, the driving torque, passive torque of the SMA wire and human-machine interaction torque have been determined. According to the torque relationship, the actual shrinkage torque of the SMA wire can be obtained by subtracting the actual value of other torques from the resultant torque. The simulation shrinkage torque can be calculated by MATLAB based on the constitutive model theory of SMA wire, and the actual value and simulation value are compared from the viewpoint with or without consideration of the

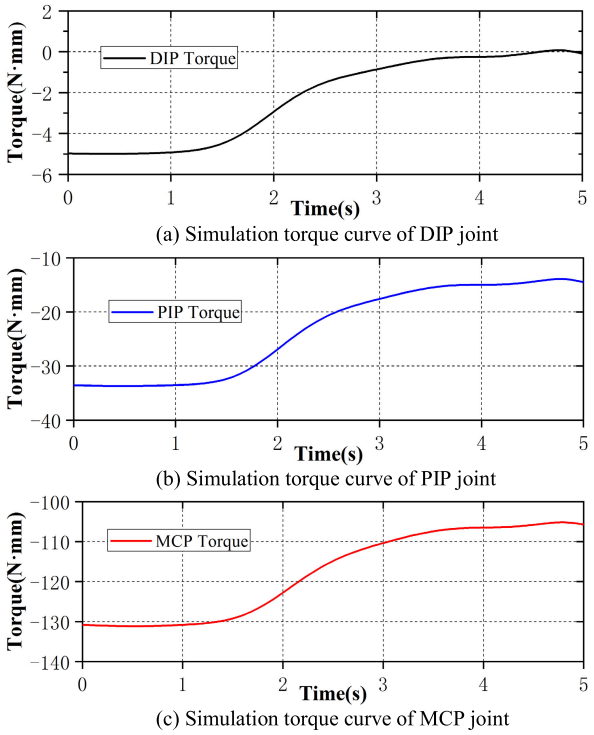

FIGURE 14. Joint driving torque simulation curve.

contact force to verify the accuracy of the coupling dynamic model. The data comparison is shown in Figure 15.

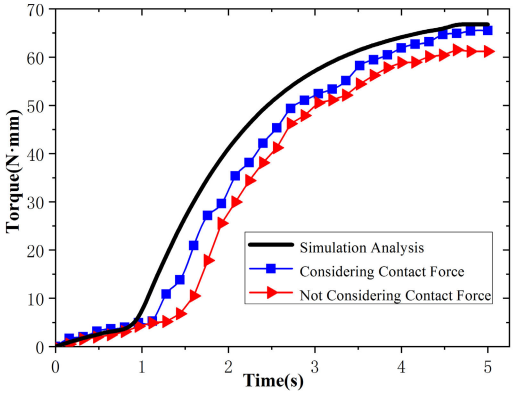

FIGURE 15. Comparison of active contraction torque of SMA wire.

It can be seen from Figure 15 that after considering the human-machine interaction contact force, the dynamic model is closer to the simulation value. Due to the hysteresis of the SMA wire, the actual shrinkage torque curve slightly lags behind the simulation curve. The martensitic transformation point of the simulation curve is 0.96 s, while the actual curve is 1.12 s. When the heating time reaches 5 s, the heating power of the SMA wire is balanced with dissipation power, the temperature tends to be stable, and the shrinkage torque simultaneously reaches the maximum value. By comparison, considering the human-machine interaction force, the actual

shrinkage torque value is more consistent with the simulation value. Because of the friction loss and geometric approximation of the joints, there are differences between the simulation value and the actual value.

By further error analysis, the error range of the dynamic model and simulation curve without considering the human-machine interaction force is between 0 and 19.57 N·mm. After considering the interaction force, the error range is between −0.74 and 10.89N·mm, and the model accuracy is improved by 7.05% on average. The accuracy of the dynamic model is remarkably improved, and the error analysis curve is shown in Figure 16.

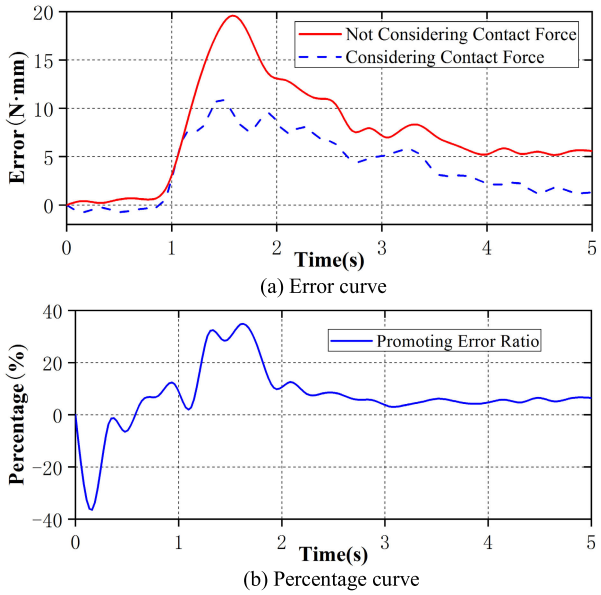

(a) Error curve

(b) Percentage curve

FIGURE 16. Model accuracy error curve.

VII. CONCLUSION

In this paper, the problem of the human-machine interaction force, which is seldom considered in the dynamic modeling of the hand rehabilitation exoskeleton equipment, is investigated. First, according to the physiological structure of the finger, the single-finger principle prototype is designed by driving the SMA wire, and the finger muscle force is analyzed based on the Hill model. Second, the exoskeleton mechanical model is established based on the virtual work principle. The interaction contact force between the finger and the exoskeleton is regarded as a spring-damping model, and the contact force equation is determined by the D-H parameters. Last, the Lagrange equation is applied to couple the muscle force, exoskeleton mechanics model and interaction force equation.

To verify the mechanical model via experiments, the bending angle trajectory is also determined. Based on the trajectory curve, the coupling dynamic model is analyzed. Multiple linear regression is applied to identify the interactive contact force model. This result shows that the elasticity coefficient k is 0.9815122N/mm and the damping c is −0.3732791N/(mm/s). From the viewpoint of whether or not the interaction contact force is considered, it is proved that the accuracy of the original dynamic model is improved by 7.05% on average.

APPENDIX

See Table 6.

TABLE 6. Abbreviations.

SMA	Shape Memory Alloy
FDP	Flex Digitorum Profundus
FDS	Flex Digitorum Superficialis
LE	Long Extenor
RI	Radial Interosseous
UI	Ulnar Interosseous
LU	Lumberic
TE	Terminal Extractor
ES	Extractor Slip
UB	Ulnar Band
RB	Radial Band
TPU	Thermoplastic Polyurethanes
PWM	Pulse Width Modulation

REFERENCES

[1] G. Kwakkel, B. J. Kollen, J. van der Grond, and A. J. H. Prevo, "Probability of regaining dexterity in the flaccid upper limb: Impact of severity of paresis and time since onset in acute stroke," *Stroke*, vol. 34, no. 9, pp. 2181–2186, Sep. 2003.

[2] S. Ueki, H. Kawasaki, S. Ito, Y. Nishimoto, M. Abe, T. Aoki, Y. Ishigure, T. Ojika, and T. Mouri, "Development of a hand-assist robot with multi-degrees-of-freedom for rehabilitation therapy," *IEEE/ASME Trans. Mechatronics*, vol. 17, no. 1, pp. 136–146, Feb. 2012.

[3] A. Wege and A. Zimmermann, "Electromyography sensor based control for a hand exoskeleton," in *Proc. IEEE Int. Conf. Robot. Biomimetics (ROBIO)*, Dec. 2007, pp. 1470–1475.

[4] P. Weiss, L. Heyer, T. F. Munte, M. Heldmann, A. Schweikard, and E. Maehle, "Towards a parameterizable exoskeleton for training of hand function after stroke," in *Proc. IEEE 13th Int. Conf. Rehabil. Robot. (ICORR)*, Jun. 2013, pp. 1–6.

[5] A. Hadi, K. Alipour, S. Kazeminasab, and M. Elahinia, "ASR glove: A wearable glove for hand assistance and rehabilitation using shape memory alloys," *J. Intell. Mater. Syst. Struct.*, vol. 29, no. 8, pp. 1575–1585, May 2018.

[6] B. B. Kang, H. In, and K.-J. Cho, "Modeling of tendon driven soft wearable robot for the finger," in *Proc. 10th Int. Conf. Ubiquitous Robots Ambient Intell. (URAI)*, Oct. 2013, pp. 459–460.

[7] U. Jeong, H. In, H. Lee, B. B. Kang, and K.-J. Cho, "Investigation on the control strategy of soft wearable robotic hand with slack enabling tendon actuator," in *Proc. IEEE Int. Conf. Robot. Autom. (ICRA)*, May 2015, pp. 5004–5009.

[8] B. B. Kang, H. Lee, H. In, U. Jeong, J. Chung, and K.-J. Cho, "Development of a polymer-based tendon-driven wearable robotic hand," in *Proc. IEEE Int. Conf. Robot. Autom. (ICRA)*, May 2016, pp. 3750–3755.

[9] H. K. Yap, B. W. K. Ang, J. H. Lim, J. C. H. Goh, and C.-H. Yeow, "A fabric-regulated soft robotic glove with user intent detection using EMG and RFID for hand assistive application," in *Proc. IEEE Int. Conf. Robot. Autom. (ICRA)*, May 2016, pp. 3537–3542.
[10] P. Polygerinos, Z. Wang, K. C. Galloway, R. J. Wood, and C. J. Walsh, "Soft robotic glove for combined assistance and at-home rehabilitation," *Robot. Auto. Syst.*, vol. 73, pp. 135–143, Nov. 2015.
[11] H. T. Di, *Mechanical Design and Analysis of Finger Rehabilitation Training Device*. Qinhuangdao, China: YanShan Univ. China, 2016.
[12] Y. Kim, S. Jung, and I. Moon, "Design of a wearable of upper-limb rehabilitation robot using paraller mechanism," in *Proc. ICROS-SICE Int. Joint Conf.*, Aug. 2009, pp. 785–789.
[13] F. Zhang, X. Wang, Y. Yang, Y. Fu, and S. Wang, "A human-machine interface software based on Android system for hand rehabilitation robot," in *Proc. IEEE Int. Conf. Inf. Autom.*, Aug. 2015, pp. 625–630.
[14] J. Wang, J. Li, Y. Zhang, and S. Wang, "Design of an exoskeleton for index finger rehabilitation," in *Proc. Annu. Int. Conf. IEEE Eng. Med. Biol. Soc.*, Sep. 2009, pp. 5957–5960.
[15] D. Hu, L. Ren, D. Howard, and C. Zong, "Biomechanical analysis of force distribution in human finger extensor mechanisms," *BioMed Res. Int.*, vol. 2014, pp. 1–9, Jul. 2014.
[16] F. E. Zajac, "Muscle and tendon: Properties, models, scaling, and application tobiomechanics and motor control," *Crit. Rev. Biomed. Eng.*, vol. 17, no. 4, pp. 359–365, 1989.
[17] L. Wang, H. Li, Z. Wang, and F. Meng, "Study on upper limbrehabilitation system based on surface EMG," *Bio-Med. Mater. Eng.*, vol. 26, no. S1, pp. 795–801, 2015.
[18] K. R. S. Holzbaur, W. M. Murray, and S. L. Delp, "A model of the upper extremity for simulating musculoskeletal surgery and analyzing neuromuscular control," *Ann. Biomed. Eng.*, vol. 33, no. 6, pp. 829–840, Jun. 2005.
[19] P. H. Kuo and A. D. Deshpande, "Contribution of passive properties of muscle-tendon units to the metacarpophalangeal joint torque of the index finger," in *Proc. 3rd IEEE RAS EMBS Int. Conf. Biomed. Robot. Biomechtron.*, Sep. 2010, pp. 288–294.
[20] N. Zhang, B.-S. Niu, H.-B. Wang, F. Chen, H. Yan, and Z.-N. Jin, "Design of active disturbance rejection controller finger rehabilitation robot structure and control system," *Sci. Technol. Eng.*, vol. 19, no. 6, pp. 166–173, 2019.
[21] V. Piccirillo, L. C. S. Góes, J. M. Balthazar, and A. M. Tusset, "Deflection control of an aeroelastic system utilizing an antagonistic shape memory alloy actuator," *Meccanica*, vol. 53, nos. 4–5, pp. 727–745, Mar. 2018.
[22] K. Tanaka, "A thermomechanical sketch of shape memory effect: One-dimensional tensile behavior," *Res Mech.*, vol. 18, no. 2, pp. 251–263, 1986.
[23] H. J. Buchner, M. J. Hines, and H. Hemami, "A dynamic model for finger interphalangeal coordination," *J. Biomech.*, vol. 21, no. 6, pp. 459–468, 1988.
[24] Y.-J. Lai, L.-J. Yeh, and M.-C. Chiu, "An experimental investigation on shape memory alloy dynamic splint for a finger joint application," *Sens. Actuators A, Phys.*, vol. 173, no. 1, pp. 210–218, Jan. 2012.

YANGWEI WANG (Member, IEEE) received the B.S. degree in mechanical engineering from the Nanjing University of Aeronautics and Astronautics, Nanjing, Jiangsu, in 2002, and the M.S. and Ph.D. degrees in mechanical engineering from the Harbin Institute of Technology, Harbin, China, in 2007 and 2011, respectively.

From 2011 to 2017, he was a Lecturer with the College of Mechanical and Electrical Engineering, Nanjing University of Aeronautics and Astronautics. Since 2017, he has been an Associate Professor with the College of Mechanical and Electrical Engineering, Northeast Forestry University, Harbin. His research interests include smart materials and robotics.

Dr. Wang is a member of the International Society of Bionic Engineering and the Chinese Society of Aeronautics and Astronautics. He is a Review Expert of the *IEEE Robotics and Automation Magazine* and the *Journal of Bionic Engineering*.

SHUFANG ZHENG received the B.S. degree in mechanical design, manufacturing, and automation from Northeast Forestry University, Harbin, in 2020, where she is currently pursuing the master's degree in mechanical engineering. Her research interests include structural design of hand rehabilitation robot, finger biomechanics, and coupling dynamics.

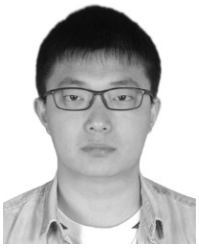

ZHICHENG SONG received the M.S. degree in mechanical engineering from Northeast Forestry University, Harbin, in 2020. He is currently pursuing the Ph.D. degree in mechanical and electronic engineering with the Nanjing University of Aeronautics and Astronautics. His main research interests include electromechanical system design of hand rehabilitation robot, bionic robot, and multibody dynamics of parallel robot.

JINGQUAN PANG, photograph and biography not available at the time of publication.

JIAN LI (Member, IEEE) received the B.S. degree in mechanical engineering from Shandong University, Jinan, China, in 2005, and the M.S. and Ph.D. degrees in mechanical engineering from the Harbin Institute of Technology, Harbin, China, in 2007 and 2011, respectively.

From 2012 to 2016, he was a Lecturer with the College of Mechanical and Electrical Engineering, Northeast Forestry University, Harbin. Since 2016, he has been an Associate Professor with the College of Mechanical and Electrical Engineering, Northeast Forestry University. His research interests include smart materials and robotics.

Dr. Li is a member of the Chinese Society of Forest and the Heilongjiang Mechanical Engineering Society. He is a Review Expert of the *Engineering Applications of Computational Fluid Mechanics and Robot*.